ChemComm

COMMUNICATION

View Article Online
View Journal | View Issue

Cite this: *Chem. Commun.*, 2025, **61**, 16572

Received 28th July 2025,
Accepted 23rd September 2025

DOI: 10.1039/d5cc04265h

rsc.li/chemcomm

Moisture-electric generator based on a facilely prepared cyanobacteria–sodium alginate–chitosan composite hydrogel

Xiuwen Wang,[a] Yunan Lin,[a] Shipu Jiao[b] and Xianhua Liu *[a]

We developed moisture-enabled electricity generation materials by loading polydopamine-modified nonwoven substrates with cyanobacteria–sodium alginate–chitosan hydrogels. Under ambient conditions, the device produced an output of 0.48 V and 2 μA. Polysaccharides and proteins released from disrupted cyanobacteria facilitated charge separation. When connected in series, the materials were able to power light-emitting diodes.

With the intensification of the global energy crisis and environmental challenges, the development of sustainable and renewable energy technologies has become a major focus in the scientific community. Among these, moisture-enabled electricity generation (MEG) has emerged as a promising green energy conversion strategy that harnesses ambient water vapor to produce electricity, offering new opportunities for the advancement of self-powered systems.[1,2]

Recent research on high-performance MEG materials focuses on systems such as carbon nanomaterials (*e.g.*, graphene oxide,[3–5] carbon nanotubes,[6] *etc.*), metal oxides,[7,8] and inorganic semiconductor materials.[9–11] However, these material systems often suffer from critical limitations. First, the fabrication processes are typically complex and energy intensive. For example, Qu *et al.*[3] explored GO-based materials for wet power generation, but the complexity of the preparation method of MEGs based on gradient GOs hinders the wide application of this method. Second, the high cost of raw materials poses economic challenges.[12] Third, and most importantly, there is a lack of environmental friendliness. For many of them, such as carbon nanotubes and other non-renewable resources or difficult to degrade components, the preparation process is characterized by high energy consumption and environmental pollution.[2] To a certain extent, these factors limit the large-scale sustainable application of MEG materials.

Therefore bio-based materials have been explored for MEG due to their renewability, environmental friendliness and biocompatibility,[13–16] but their performance enhancement often relies on additional functionalization modifications or complex processing techniques, which may increase the cost and environmental burdens.[12] For instance, Liu *et al.*[17] developed a MEG incorporating protein nanofibrils derived from milk β-lactoglobulin, but the preparation process is complicated, which is not conducive to dissemination. Therefore, it is of practical significance to develop a new bio-based MEG material with a simpler preparation process, lower cost, and outstanding environmental friendliness.

Cyanobacteria, a widely available photosynthetic microorganism, possess cell walls enriched with a variety of natural polysaccharides, proteins, and electrically charged groups, such as carboxyl (–COOH) and amino ($–NH_2$) groups.[18] Previous studies have demonstrated that these biological components may exhibit ion migration and proton conductivity in aqueous environments.[19,20] However, pure microalgae-based materials often suffer from poor mechanical strength and weak interfacial adhesion, which significantly limits the output stability of the resulting devices.[21] To address this challenge, sodium alginate (SA) and chitosan (CS), two widely available and biodegradable natural polysaccharides, have been explored as effective composite carriers due to their excellent biocompatibility, biodegradability, low cost, and simple and readily available preparation methods.[13,22,23] Combining biological components of cyanobacteria with stabilized hydrogel networks formed by SA/CS provides a possible way to design functional composites responsive to humidity.

We developed a MEG device using a cyanobacteria-SA/CS composite hydrogel. The core structure features a cyanobacteria-embedded SA/CS hydrogel layer on a PDA-modified nonwoven substrate (Fig. 1a). PDA enhances substrate-hydrogel adhesion and introduces hydrophilic groups that boost moisture adsorption *via* hydrogen bonding.[24] The fabrication involves simple mixing, coating, and ionic crosslinking (Ca^{2+}/CS) with low-cost bio-based materials under mild conditions. This CSC-MEG device

[a] *School of Environmental Sciences and Engineering, Tianjin University, Tianjin 300072, China. E-mail: lxh@tju.edu.cn*
[b] *Center for Sensor Technology of Environment and Health, School of Environment, Tsinghua University, Beijing, 100084, China*

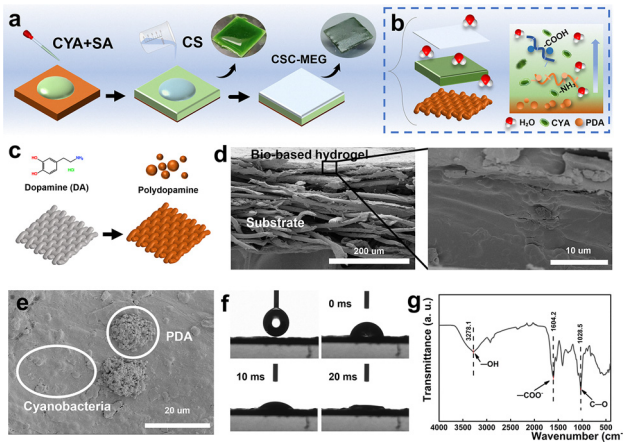

Fig. 1 Preparation and characterization of the CSC-MEG. (a) Schematic illustration of the fabrication process of the CSC-MEG. (b) The three-layer structure and composition of the CSC-MEG. (c) Representation of the PDA-modified non-woven fabric substrate. (d) Cross-sectional SEM image of the CSC-MEG and enlarged SEM image of the bio-based hydrogel membrane on the CSC surface. (e) SEM image of the CSC-MEG surface. (f) Contact angle between water and the CSC-MEG. (g) FTIR spectra of the CSC-MEG surface.

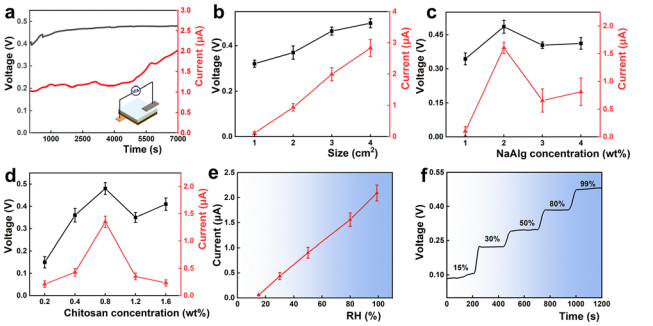

Fig. 2 Electrical output of the CSC-MEG. (a) Curves of V_{oc} and I_{sc} over time for CSC-MEG at RH = 90% and 25 °C. Effects of (b) size, (c) SA concentration, (d) CS concentration, and (e) and (f) humidity on the electrical outputs of CSC-MEG.

exhibits excellent moisture responsiveness: adsorbed water diffuses through the hydrogel membrane (Fig. 1b), generating an open-circuit voltage (V_{oc}) of 0.48 V and a short-circuit current (I_{sc}) of 2.0 μA at 90% relative humidity (RH) (3 × 3 cm^2 device).

The fabrication process of the CSC-MEG is as follows: cyanobacterial cells were first dispersed in a SA solution, and the resulting mixture was drop-cast onto a PDA-modified substrate (Fig. 1c). Subsequent crosslinking with a $CaCl_2$ solution formed the cyanobacteria-SA hydrogel, which was then immersed in a CS solution for further crosslinking to obtain the final CSC-MEG device. Electrochemical performance data were measured in a humidity-controlled box (Fig. S1).

Material characterization results are summarized as follows: cross-sectional SEM imaging of CSC-MEG (Fig. 1d) revealed a cyanobacteria-composite hydrogel film with a thickness of ≈10 μm coating the PET substrate. Surface SEM imaging (Fig. 1e) showed granular cyanobacterial cells embedded within the hydrogel matrix alongside PDA-derived structures. Excellent hydrophilicity is crucial for efficient MEG. Contact angle measurements (Fig. 1f and Fig. S2) demonstrated an initial water contact angle of 79.9° on the CSC-MEG surface, which rapidly decreased to 41.8° within a very short timeframe (<10 ms) and achieved complete wetting (contact angle ≈ 0°) within 20 ms, confirming its superhydrophilic surface properties. The ion dissociation characteristics were evaluated by measuring the zeta potential.[25] At neutral pH (7.05 ± 0.04), the CSC-MEG surface possessed a stable negative charge (−17.64 ± 0.44 mV). This negative surface charge facilitates the enrichment of protons (H^+) at the gas–solid interface, thereby creating a higher potential at the top electrode and driving a sustained potential difference. Fourier transform infrared (FTIR) spectroscopy (Fig. 1g) further confirmed the presence of abundant hydrophilic functional groups—such as hydroxyl (–OH), amino (–NH_2), and carboxyl (–COOH) groups—on the CSC-MEG surface. These functional groups play a critical role in facilitating efficient moisture capture and promoting ion migration.

The power output performance of the CSC-MEG was first evaluated. Under high relative humidity conditions (RH = 90%), both the V_{oc} and I_{sc} of the device gradually increased over time, eventually reaching peak values of 0.48 V and 0.2 μA, respectively (Fig. 2a). Meanwhile, we also evaluated the performance using different electrodes and found that the changes in performance were not significant (Fig. S4). To investigate the key factors influencing the MEG performance of CSC-MEG, a series of single-variable experiments were conducted. Given that previous studies have reported the significant impact of device dimensions on MEG efficiency,[26] the electrical performance of CSC-MEG devices with varying sizes (1 × 1 cm^2, 2 × 2 cm^2, 3 × 3 cm^2, 4 × 4 cm^2) was measured (Fig. 2b). All data were recorded after the electrical performance reached a steady state. The results demonstrated that both V_{oc} and I_{sc} increased with enlarging device size. To rule out the influence of the photosynthesis of cyanobacterial cells, we conducted a control experiment under conditions of light and darkness (Fig. S5).

The SA/CS crosslinking concentration critically influences electrical performance (Fig. 2c and d). When varying SA concentration (1–4 wt%) at fixed CS (0.8 wt%), both V_{oc} and I_{sc} peaked at 2 wt% SA before declining at higher concentrations. Similarly, optimizing CS concentration (0.2–1.6 wt%) at 2 wt% SA revealed identical trends. This performance decay stems from excessive crosslinking density at higher concentrations, which reduces hydrogel porosity and impedes water/ion transport, ultimately diminishing MEG efficiency.

To confirm the dependence of CSC-MEG on ambient moisture, a series of humidity-response tests were conducted. We placed the CSC-MEG in a dry environment with a relative humidity (RH ≈ 0%), and almost no electrical signals were detected (Fig. S5). We then systematically evaluated the device performance under a range of relative humidity (RH) levels, from 15% to 99%, using a controlled environmental setup. As shown in Fig. 2e and f, the V_{oc} and I_{sc} increased progressively with humidity. These results demonstrate the critical role of

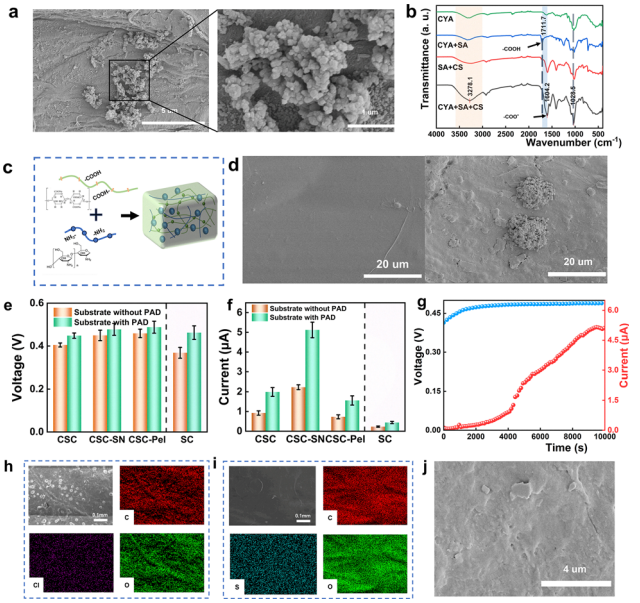

Fig. 3 Mechanistic investigation of the CSC-MEG. (a) The SEM image of PDA attached to the nonwoven substrate. (b) FTIR spectra of the four samples: CYA, CYA + SA, SA + CS, and CYA + SA + CS. (c) Schematic diagram of crosslinking between SA and CA. (d) Comparison of SEM images between SC and CSC. (e) Open-circuit voltages of the four samples. (f) Open-circuit currents of the four samples: CSC, CSC-SN, CSC-Pel, and SC. (g) Curves of current and voltage over time for CSC-SN at RH = 90%. (h) C, Cl, and O mapping of the CSC film. (i) Carbon, oxygen, and sulfur mapping of the CSC-SN film. (j) Surface SEM image of CSC-SN.

moisture in powering the CSC-MEG, with both the voltage and current outputs increasing with RH.

We first discussed the effect of PDA modification on the moisture adsorption capability of the non-woven fabric substrate. Materials without PDA substrates were prepared, and Fig. 3a shows the SEM image of PDA attached to the nonwoven substrate. The enhanced moisture adsorption capability of the PDA-modified substrates is attributed to the abundant oxygen-containing functional groups in the PDA films, such as hydroxyl (C–OH) and carbonyl (C═O) groups, which can form hydrogen bonds with water molecules, enabling rapid and efficient water adsorption.[27]

To examine the effect of cyanobacteria, SA, and CS on moisture absorption, four samples (CYA, CYA + SA, SA + CS, and CYA + SA + CS) were fabricated for FTIR analysis on uncoated substrates to exclude PDA interference. FTIR spectra (Fig. 3b) confirmed SA-CS electrostatic cross-linking: in CYA + SA + CS, the disappearance of the protonated carboxyl peak (1711.7 cm^{-1}) and emergence of an ionized carboxyl peak (1604 cm^{-1}) verify SA ($–COO^-$) complexation with protonated CS ($–NH_3^+$), forming a stable PEC (Fig. 3c). Concurrently, significant broadening/red-shift of the O–H peak (3278 cm^{-1}) and intensification of the 1028.5 cm^{-1} peak demonstrate enhanced hydrogen bonding networks between CS ($–NH_2$/–OH), SA, and cyanobacterial polysaccharides. These synergistic interactions establish heterogeneous hydrated proton conduction pathways. SEM (Fig. 3d) further revealed CYA + SA + CS's aggregated protrusions *versus* smoother SA + CS, where increased surface roughness provides additional active sites for atmospheric moisture adsorption, boosting the power generation efficiency.[12]

In addition, to gain further insight into the generator system of CSC-MEG, we propose two possible synergistic contributions from cyanobacteria during the moisture power generation process: First, the nanofibrous architecture of the cyanobacterial cell walls may integrate with the three-dimensional network of SA, forming a hierarchical porous structure that facilitates the penetration of water molecules and directional migration of ions.[28–30] Second, proteins, polysaccharides and other substances rich in hydrophilic groups in cyanobacterial cells ionize water molecules and produce free-moving H (H from hydroxyl or carboxyl groups, *etc.*) during the power generation process, thus enhancing power generation performance.[17,29] To elucidate the underlying mechanism, cyanobacteria cells were subjected to ultrasonication for disruption. The resulting supernatant (primarily containing soluble intracellular components such as proteins, polysaccharides, and amino acids) and pellet (primarily containing cell wall fragments, intact cells, and large organelles) were separately incorporated into the MEG materials, designated as CSC-SN and CSC-Pel, respectively. A control sample without cyanobacteria was also prepared and designated as SC. The sample prepared by the original method was designated as CSC. Detailed experimental procedures are provided in the SI.

To quantify the performance enhancements, V_{oc} and I_{sc} of the four samples (CSC, CSC-SN, CSC-Pel, SC) and the PDA-modified samples were measured, as shown in Fig. 3e and f. For the PDA-modified samples, the open-circuit current and short-circuit voltage of CSC-MEG were higher than those without PDA, confirming that PDA enhances moisture adsorption (consistent with the findings by Li *et al.*[27]). For the four composite samples, the corresponding power outputs were 0.89 μW, 2.44 μW, 0.76 μW, and 0.20 μW, respectively. These results demonstrate a significant enhancement in moisture adsorption attributable to the integration of cyanobacteria within the composite hydrogel system.

Furthermore, cyanobacteria-derived soluble components (*e.g.*, proteins/polysaccharides in the supernatant, CSC-SN) dominate the MEG process, evidenced by CSC-SN's significantly higher power output *versus* CSC-Pel and SC (Fig. 3e and f). Elemental mapping reveals CSC-SN's enrichment in N/S (indicative of ion-migrating biomolecules like proteins), contrasting with CSC's C/O dominance (Fig. 3h and i). SEM morphology (Fig. 3j) further supports this, collectively confirming the soluble components' key role in enhancing ion migration and power generation.

We also evaluated the long-term power generation performance of CSC-MEG. As shown in Fig. 4a, the device operated continuously for over 500 minutes with negligible voltage decay. As with other DC power supplies, the output of CSC-MEG devices can be enhanced through series and parallel configurations. As illustrated in Fig. 4b and c, the output voltage of CSC can be increased by series connection, while

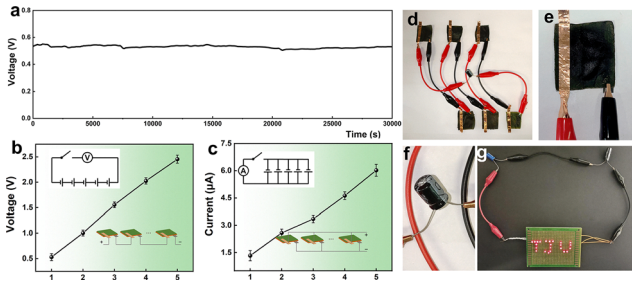

Fig. 4 Application of a CSC-MEG. (a) V_{oc} of a CSC-MEG in a continuous 30 000 s. (b) V_{oc} of 1, 2, 3, 4, and 5 series-connected CSC-MEGs. (c) I_{sc} of 1, 2, 3, 4, and 5 parallel-connected CSC-MEGs. (d) Six series-connected CSC-MEGs charging a capacitor under ambient relative humidity of ~90% RH (20 °C± 5 °C). (e) A single CSC-MEG. (f) A small capacitor (3.3 F, 2.7 V). (g) The charged capacitor can light up a Tianjin University pattern composed of 24 LEDs.

V_{oc} almost increases linearly with the number of series connections, reaching ~2.5 V with five CSC-MEG units. The pattern is similar when CSC-MEG devices are connected in series, with I_{sc} increasing almost linearly with the number of parallel connections, and five parallel CSC-MEG devices are capable of generating ~6.0 μA of output current. To simulate practical conditions, we assembled a power generation module consisting of a combination of 6 CSC-MEG devices (Fig. 4d and e) and tested under a high-humidity environment (RH = 90%). The module successfully charged a rechargeable capacitor (3.3 F, 2.7 V) (Fig. 4f), and two such capacitors connected in series were able to power a commercial LED light, as shown in Fig. 4g. CSC-MEG is flexible, and its applications can be further expanded in the future (Fig. S6).

It is important to emphasize that the working mechanism of the CSC-MEG differs fundamentally from evaporation-driven power generation. In the CSC-MEG, the power output primarily arises from water vapor adsorption and the subsequent formation of a hydration layer, rather than from phase transitions or thermal energy input. The process is isothermal and chemical-potential-driven. The key evidence is the direct proportionality of the electrical output to the ambient relative humidity (Fig. 2e and f) and the absence of any output in a dry atmosphere. In contrast, evaporation-induced power generation typically relies on liquid water sources and thermal gradients to sustain vapor flow. Our device operates directly in ambient vapor, leveraging the natural humidity gradient to drive ion dissociation and proton diffusion within the hydrogel, without the need for evaporation.

This study demonstrates a moisture-electric generator based on a cyanobacteria-SA-CS composite hydrogel. The optimized device (3×3 cm^2) achieves outputs of 0.48 V and 2.0 μA at 90% RH with humidity-dependent responsiveness (0.10–0.49 V for 15–99% RH). The material exhibits robust stability (>500 min), and scalable power generation *via* series/parallel connections (*e.g.*, 2.5 V from 5-series units) enables practical applications. This work offers a sustainable pathway for eco-friendly moisture-enabled energy harvesting.

Conflicts of interest

There are no conflicts to declare.

Data availability

The data supporting this article have been included as part of the article and its supplementary information (SI). Supplementary information: experimental section and Fig. S1–S7. See DOI: **https://doi.org/10.1039/d5cc04265h**.

Notes and references

1 D. Shen, W. W. Duley, P. Peng, M. Xiao, J. Feng, L. Liu, G. Zou and Y. N. Zhou, *Adv. Mater.*, 2020, **32**, 2003722.
2 J. Tan, X. Wang, W. Chu, S. Fang, C. Zheng, M. Xue, X. Wang, T. Hu and W. Guo, *Adv. Mater.*, 2024, **36**, 2211165.
3 F. Zhao, H. Cheng, Z. Zhang, L. Jiang and L. Qu, *Adv. Mater.*, 2015, **27**, 4351–4357.
4 G. Xue, Y. Xu, T. Ding, J. Li, J. Yin, W. Fei, Y. Cao, J. Yu, L. Yuan, L. Gong, J. Chen, S. Deng, J. Zhou and W. Guo, *Nat. Nanotechnol.*, 2017, **12**, 317–321.
5 F. Zhao, Y. Liang, H. Cheng, L. Jiang and L. Qu, *Energy Environ. Sci.*, 2016, **9**, 912–916.
6 S. Chen, H. Xia and Q.-Q. Ni, *Carbon*, 2022, **194**, 104–113.
7 D. Shen, M. Xiao, G. Zou, L. Liu, W. W. Duley and Y. N. Zhou, *Adv. Mater.*, 2018, **30**, 1705925.
8 R. Gogoi, P. Garg, P. P. Das, A. K. Rajak, N. Nath, S. Roy and K. Raidongia, *Nano Energy*, 2024, **131**, 110187.
9 D. Shen, M. Xiao, G. Zou, L. Liu, W. W. Duley and Y. N. Zhou, *Adv. Mater.*, 2018, **30**, 1705925.
10 Y. Qin, Y. Wang, X. Sun, Y. Li, H. Xu, Y. Tan, Y. Li, T. Song and B. Sun, *Angew. Chem.*, 2020, **132**, 10706–10712.
11 J. Chen, P. He, T. Huang, D. Zhang, G. Wang, S. Yang, X. Xie and G. Ding, *Nano Energy*, 2021, **90**, 106593.
12 Z. Sun, X. Wen, L. Wang, D. Ji, X. Qin, J. Yu and S. Ramakrishna, *eScience*, 2022, **2**, 32–46.
13 J. Deng, C. Liu, X. Wang and L. Qiu, *Nano Energy*, 2025, **142**, 111155.
14 S. Mandal, S. Roy, A. Mandal, T. Ghoshal, G. Das, A. Singh and D. K. Goswami, *ACS Appl. Electron. Mater.*, 2020, **2**, 780–789.
15 H. He, J. Zhang, J. Pan, Z. Wang, M. Deng, X. Liu and F. Fu, *ACS Appl. Energy Mater.*, 2024, **7**, 2980–2988.
16 Q. Lyu, B. Peng, Z. Xie, S. Du, L. Zhang and J. Zhu, *ACS Appl. Mater. Interfaces*, 2020, **12**, 57373–57381.
17 J. Liu, L. Huang, W. He, X. Cai, Y. Wang, L. Zhou and Y. Yuan, *Nano Energy*, 2022, **102**, 107709.
18 E. Hoiczyk and A. Hansel, *J. Bacteriol.*, 2000, **182**, 1191–1199.
19 S. Xu, Y. Zhao, S. Jiao, Z. Wang, Z. Yu, C. Sun and X. Liu, *Adv. Sci.*, 2024, **11**, 2400856.
20 G. Ren, Z. Wang, B. Zhang, X. Liu, J. Ye, Q. Hu and S. Zhou, *Nano Energy*, 2021, **89**, 106361.
21 S. Tazikeh, S. Zendehboudi, S. Ghafoori, A. Lohi and N. Mahinpey, *J. Environ. Chem. Eng.*, 2022, **10**, 107863.
22 X. Jiang, N. Xiang, H. Zhang, Y. Sun, Z. Lin and L. Hou, *Carbohydr. Polym.*, 2018, **186**, 377–383.
23 S. Yang, L. Zhang, J. Mao, J. Guo, Y. Chai, J. Hao, W. Chen and X. Tao, *Nat. Commun.*, 2024, **15**, 3329.
24 Y. Li, L. Huang, W. He, Y. Chen and B. Lou, *Polymers*, 2018, **10**, 570.
25 H. Wang, Y. Sun, T. He, Y. Huang, H. Cheng, C. Li, D. Xie, P. Yang, Y. Zhang and L. Qu, *Nat. Nanotechnol.*, 2021, **16**, 811–819.
26 X. Liu, T. Ueki, H. Gao, T. L. Woodard, K. P. Nevin, T. Fu, S. Fu, L. Sun, D. R. Lovley and J. Yao, *Nat. Commun.*, 2022, **13**, 4369.
27 L. Li, Z. Chen, M. Hao, S. Wang, F. Sun, Z. Zhao and T. Zhang, *Nano Lett.*, 2019, **19**, 5544–5552.
28 J. Zhou, Z. Ren, X. Cui, X. Liu and X. Lu, *Adv. Energy Mater.*, 2025, 2404840.
29 M. Li, L. Zong, W. Yang, X. Li, J. You, X. Wu, Z. Li and C. Li, *Adv. Funct. Mater.*, 2019, **29**, 1901798.
30 H. Zhong, S. Wang, Z. Wang and J. Jiang, *Chem. Eng. J.*, 2024, **486**, 150203.